

Kinematics of High-Velocity Stars Utilizing LAMOST and Gaia DR3 Archives within 100 kpc

W. H. Elsanhoury^{1,2} 

¹*Physics Department, College of Science, Northern Border University, Arar,
Saudi Arabia.*

²*Astronomy Department, National Research Institute of Astronomy and
Geophysics (NRIAG), 11421 Helwan. Cairo, Egypt.
(E-mail: elsanhoury@nriag.sci.eg & elsanhoury@nbu.edu.sa)*

Received: XX XX, XXXX; Accepted: XX XX, XXXX

Abstract. The kinematic parameters identified from high-velocity stars situated within ~ 100 kpc are examined and analyzed. We included three high-velocity programs comprising 591, 87, and 519 stars as a function of distances ranging from 0.10 to nearly 109 kpc. In this analysis, we will determine the spatial velocities (U , V , W) in galactic coordinates along with their velocity dispersion (σ_1 , σ_2 , σ_3), the convergent point (A_o , D_o), and therefore, the solar motion (S_\odot). In conclusion, we are calculating the first Oort constant ($A = 11.94 \pm 0.29 \text{ km s}^{-1} \text{ kpc}^{-1}$) and the second one (i.e., $B = -17.78 \pm 0.24 \text{ km s}^{-1} \text{ kpc}^{-1}$), the angular rotation rate $|A-B| = 25.07 \pm 5.01 \text{ km s}^{-1} \text{ kpc}^{-1}$, and the average rotational velocity $V_o = 243.72 \pm 15.61 \text{ km s}^{-1}$.

Key words: High-velocity stars – Gaia DR3 – Kinematics – Oort constants.

1. Introduction

The stars known as high-velocity stars (HiVels) travel through space at substantially faster rates than the average Milky Way (MW) Galaxy star. These objects are special in astronomy study since they can reach speeds of thousands or even hundreds of kilometers per second. In the disk region, almost all the stars in our Galaxy rotate around the galactic center at a normal velocity of 200–240 km s^{-1} (Bovy et al., 2012; Huang et al., 2016; Eilers et al., 2019). An alternative indirect estimate of both the circular velocity (V_o) and the escape velocity (V_{esc}) at which the stars in the solar neighborhood would have sufficient energy to completely escape from our Galaxy’s gravitational field can be obtained from the kinematic properties of the halo-population stars that have been observed to have the largest space velocities to the Sun (i.e., the extreme HiVels).

Including the Gaia DR3, Large Sky Area Multi-Object Fiber Telescope (LAMOST, Cui et al. (2012)) galactic surveys, and spectroscopic observations

from large-scale galactic surveys (SEGUE, (Yanny et al., 2009; Rockosi et al., 2022)) have demonstrated the existence of HiVels in our Galaxy. Among these, a few are even hypervelocity stars (HVSs), meaning that their V_{esc} is less than their overall galactocentric velocities (V_{GSR}), and almost all HiVels have low luminosity ($M_G \sim 10$ mag).

In the halo, they exhibit tens of kilometers per second (Xue et al., 2008; Huang et al., 2016), especially when a star approaches or even exceeds the Galaxy’s escape velocity at its position. HiVels indicate the presence of extreme dynamical and astrophysical processes (Hills, 1988; Yu & Tremaine, 2003; Bromley et al., 2006; Abadi et al., 2009; O’Leary & Loeb, 2008; Capuzzo-Dolcetta & Fragione, 2015; Marchetti et al., 2019). The finding of such rare objects offers a valuable tool for investigating the MW’s mass distribution, particularly its dark component (Gnedin et al., 2005; Rossi et al., 2017; Contigiani et al., 2019), because they travel large distances across it (Gnedin et al., 2005; Kenyon et al., 2008), and their trajectories can also be used to probe the shape of the Galaxy’s dark matter halo (Bromley et al., 2006; Yu & Madau, 2007). The study of stellar motion and the dynamics of the MW Galaxy reveals a relationship between HiVels and the Oort constants (A & B), where HiVels offer special test cases for comprehending extreme stellar motions both inside and outside of the Galaxy.

HiVels and HVSs can be divided into four subclasses, each with a distinct origin of these high velocities; i) black hole ejection (BHE): As a result of tidal interaction between a close stellar binary system and a supermassive black hole (SMBH) in the Galaxy, a process known as the "Hills mechanism," the so-called HVSs (with velocities even greater than 1000 km s^{-1}) were first predicted from theoretical arguments of Hills (1988). Extending the Hills mechanism allows for the ejection of HVSs and HiVels, ii) supernova explosions (SNEs), can cause significant disruption to binary systems and induce their companion stars to become HiVels or HVSs. Examples of such explosions include core-collapse and thermonuclear supernova explosions (SNe) (Blaauw, 1961; Portegies Zwart, 2000; Justham et al., 2009; Wang & Han, 2009; Pakmor et al., 2013; Zubovas et al., 2013; Shen et al., 2018; Neunteufel, 2020; Bauer et al., 2019). Generally, stars with velocities of no more than $300\text{--}400 \text{ km s}^{-1}$ cannot be ejected by core-collapse SNEs (Portegies Zwart, 2000), iii) dynamic ejection mechanism (DEM) as proposed by Poveda et al. (1967), into which a possible explanation for the runaway stars in the galactic Outer Belt. This process involves the expulsion of runaway stars from young stellar clusters because of close stellar interactions. This mechanism often achieves a maximum kick velocity of around $300\text{--}400 \text{ km s}^{-1}$, which is the result of collisions between two close binaries (Leonard & Duncan, 1990; Leonard, 1991; Gvaramadze et al., 2009), and iv) tidal stripping from dwarf galaxies (TSD): In this scenario, stars can be rapidly removed from a dwarf Galaxy that is pericentrically passing through a region where the MW gravity field is causing tidal disruption Abadi et al. (2009). According to Piffi et al. (2011), runaway stars in this mechanism must be expelled by a large dwarf Galaxy ($> 10^{10} M_{\odot}$).

The study aims to examine and report the spatial structures, kinematics of the HiVels, including their velocity ellipsoid motion characteristics, parameters characterizing the local rotational properties of our Galaxy such as Oort’s constants A and B . In the context of our ongoing investigations into stellar associations, we present velocity ellipsoid parameters for three Program stars as a function of distances (d), i.e., Program I (591 stars; $0.10 \leq d(\text{kpc}) \leq 15.40$), Program II (87 stars; $0.30 \leq d(\text{kpc}) \leq 108.64$), and Program III (519 stars; $0.29 \leq d(\text{kpc}) \leq 16.44$). Moreover, determination of the equatorial coordinates for convergent points (i.e., A_o , D_o) with AD-chart method. Finally, we computed the MW Galaxy’s local differential rotation close to the Sun, i.e., the Oort constants (A & B) based on observed velocities of three considered Program stars.

The remainder of this article is structured as follows: Section 2 provides the selected data considered in this analysis. Section 3 details the computational methods, including velocity ellipsoid parameters and the convergent point Section 4 deals with the galactic rotational constants. We close finally with discussion and conclusions in Section 5.

2. Selected data

Large Sky Area Multi-Object Fiber Spectroscopic Telescope (LAMOST), also named the “Guo Shou Jing” Telescope (Cui et al., 2012) is a 4-m Schmidt spectroscopic survey telescope specifically developed to study four thousand targets per exposure in a field of view roughly 5° in diameter (Cui et al., 2012; Luo et al., 2012; Feltzing et al., 2014). LAMOST spectra have a resolution of ~ 1800 with a wavelength range of 3800–9100 Å. In March 2020, 10,608,416 spectra in DR7¹ (Lei et al., 2020) were made accessible by LAMOST.

The third major data release from the European Space Agency’s (ESA) Gaia mission, which aspires to provide the most precise three-dimensional map of the Milky Way, is called Gaia Data Release 3 (hereafter DR3) (Gaia Collaboration et al., 2023). Gaia is an astrometry expedition that was launched in 2013 to determine the locations, distances, movements, and other characteristics of over one billion stars and other celestial objects. Released on June 13, 2022, DR3 represents a major update to the earlier Gaia data releases (DR1 and DR2).

Understanding stars’ physical characteristics and chemical makeup. Moreover, detailed astrometric parameters like equatorial coordinate system (α , δ), parallaxes (π ; mas), movements within the MW as well-known the proper motion (PM; mas yr^{-1}) components in right ascension and declination ($\mu_\alpha \cos \delta$, μ_δ) for roughly 470 million stars, and radial velocities (V_r ; km s^{-1}) for 34 million stars, DR3 is a rich source of stellar data and provides photometric across three broadband filters: the G band (330–1050 nm), the Blue Prism (G_{BP} : 330–680 nm), and the Red Prism (G_{RP} : 630–1050 nm) for sources brighter than 21 mag.

¹<http://dr7.lamost.org/>

Common errors in the photometric observations throughout these three bands with $G \leq 20$ magnitudes are approximately 0.30 magnitudes and are increased for fainter stars (approaching $G = 21$). DR3 can measure PM for the bright stars ($G \leq 15$) with remarkable accuracy, frequently to within ~ 0.02 to 0.03 mas yr $^{-1}$. With uncertainties of about 1.00 mas yr $^{-1}$ or exceed for fainter stars ($G = 20$), but still yields useful motion data. The uncertainty limit in parallax is about 0.02 to 0.03 mas for $G < 15$ mag, ~ 0.07 mas for $G = 17$ mag, ~ 0.50 mas for $G = 20$ mag, and ~ 1.30 mas for $G = 21$ (Gaia Collaboration et al., 2023). The astrometric accuracy of DR3 is significantly better than that of DR2, with PM accuracy being doubled and parallax accuracy being roughly 1.5 times higher. Furthermore, astrometric inaccuracies in parallax measurements were reduced by 30-40%, while accurate motion measurements were improved by 2.5 times.

Li et al. (2021) reported on approximately 591 HiVels in the galactic halos with three-dimensional velocities in the galactic rest frame larger than 445 km s $^{-1}$ that were chosen from over 10 million spectra of Data Release 7 of the Large Sky Area Multi-object Fiber Spectroscopic Telescope (LAMOST DR7) and the second Gaia data release (Gaia DR2, Gaia Collaboration et al. (2016)).

According to the fifth data release of the V_r Experiment survey (RAVE DR5, (Kunder et al., 2017)), the twelfth data release of the Sloan Digital Sky Survey (SDSS DR12, (Alam et al., 2015)), the eighth data release of Large Sky Area Multi-Object Fiber Telescope (LAMOST DR8, (Wang et al., 2022)), sixteenth data release of The Apache Point Observatory Galactic Evolution Experiment (APOGEE DR16, (Majewski et al., 2017)), second data release of the Galactic Archaeology (GALAH DR2, (De Silva et al., 2015)), and Early Data Release 3 (Gaia EDR3), Li et al. (2023) presents about 88 HiVels by large-scale galactic surveys.

With crossmatch between DR3 and precise V_r with other large-scale galactic surveys, such as GALAH DR3 (De Silva et al., 2015; Buder et al., 2021), LAMOST DR10 (Yanny et al., 2009; Zhao et al., 2012), RAVE DR6 (Steinmetz et al., 2020), APOGEE DR17 (Majewski et al., 2017), Liao et al. (2024) presents about 591 HiVels of the Large Magellanic Cloud (LMC).

In what follows, we attention to bold here and report in our analysis three Programs (I, II, and III) of halo HiVels as a function of distances and lags between a few parsecs till ~ 100 kpc.

The most recent data from DR3 was used to update and enhance Programs I, II, and III. To ensure data consistency crossmatches were carried out using software that was based on the Tool for OPERations on Catalogues And Tables (TOPCAT) and Starlink Tables Infrastructure Library (STIL; Taylor (2005)). This tool has several options for modifying astronomical catalogs and is especially reliable when examining tabular data within a given range ($0 < x < 1$).

- (i) The Program I mainly aim to comprehend the galactic and kinematic characteristics of about 591 HiVels (Li et al., 2021) with LAMOST and Gaia

DR3 located ($0.10 \leq d(\text{kpc}) \leq 15.40$).

- (ii) Program II was set for 87 HiVels who are ejected from the galactic center with large-scale galactic surveys (Li et al., 2023) with DR3, LAMOST, SDSS, and other large-scale surveys combining astrometric and spectroscopic data within ($0.30 \leq d(\text{kpc}) \leq 108.64$). The missed one of 88 stars is HVS23 ($\alpha = 240^\circ.537580$, $\delta = 0^\circ.912272$) into which there is no Gaia DR3 identification number and no proper motions data in both directions, therefore, we neglect it from this Program set.
- (iii) Program III was set and updated via DR3 sources for 519 HiVels influenced by LMC's gravitational potential Liao et al. (2024) in the range of ($0.29 \leq d(\text{kpc}) \leq 16.44$).

Table 1 presents the fundamental parameters of these three Programs of HiVels (Li et al., 2021, 2023; Liao et al., 2024), respectively. The distribution of selected stars across the sky is shown in Figure 1 with almost random directions of velocity vectors. Figure 2 presents the V_r distribution as a function of galactic longitude (l°) for all halo HiVels observed in our considered three Programs (I, II, and III).

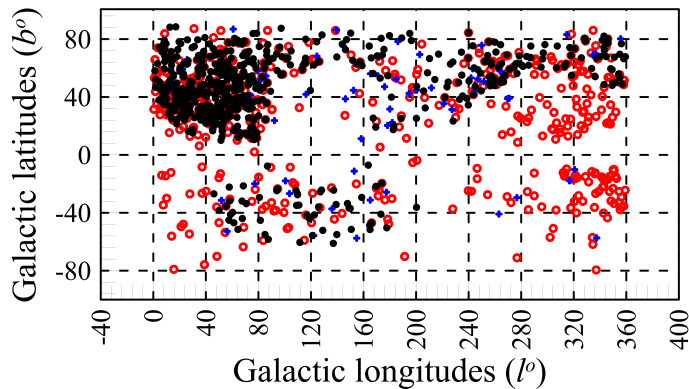


Figure 1. Distribution of HiVels in the galactic coordinate system (l, b). Program I: black closed circles (591 stars), Program II: blue closed pluses (87 stars), and Program III: red open circles (519 stars).

3. VEPs and CP

3.1. Velocity Ellipsoid Parameters (VEPs)

A equatorial-galactic transformation matrix based on the SPECFIND v2.0 catalog of radio continuum spectra (see Eq. (14); Liu et al. (2011)) was used to

Table 1. The fundamental parameters of the three Programs I, II, and III of HiVels adopted by Li et al. (2021, 2023), and Liao et al. (2024), respectively.

No.	Gaia DR3 ID	Ra. (deg.)	Dec. (deg.)	$V_r \pm \sigma_{V_r}$ (Km s ⁻¹)
Program I: $N = 591$ stars				
$0.10 \leq d(\text{kpc}) \leq 15.40$				
1	1383279090527227264	240.3375	41.1668	-184 ± 5.00
2	1570348658847157888	193.4372	55.0581	-230 ± 15.00
3	966594450238136704	102.4834	46.8368	-80 ± 6.00
.
.
.
591	1272009269712167680	229.6719	28.3365	-147 ± 12.00
Program II: $N = 87$ stars				
$0.30 \leq d(\text{kpc}) \leq 108.64$				
1	255667999133782348	12.3624	7.1290	-345.37 ± 9.48
2	2801887851883799936	12.5096	21.4207	-32.94 ± 14.38
3	2510946771548268160	29.3032	1.1937	217 ± 2.26
.
.
.
87	2872564390598678016	352.2706	33.0032	237.3 ± 6.40
Program III: $N = 519$ stars				
$0.29 \leq d(\text{kpc}) \leq 16.44$				
1	6087590373666222080	201.7684	-44.5009	328.84 ± 1.19
2	6098873935647575552	220.6412	-44.5675	163.15 ± 0.71
3	6135358205355639424	193.4286	-44.9466	203.66 ± 0.32
.
.
.
519	4421621689671197568	229.5736	2.1771	-54.16 ± 0.82

derive the spatial velocity components (U , V , and W ; km s⁻¹) of HiVels in galactic coordinates with the aid of the calculated space velocity components (V_x , V_y , and V_z ; km s⁻¹) at distances (d_i ; pc) from the Sun as given in Eqs. (4, 5, and 6). Therefore,

$$U = -0.0518807421V_x - 0.8722226427V_y - 0.4863497200V_z \quad (1)$$

$$V = 0.4846922369V_x - 0.4477920852V_y + 0.7513692061V_z, \quad (2)$$

$$W = -0.8731447899V_x - 0.1967483417V_y + 0.4459913295V_z \quad (3)$$

where

$$V_x = -4.74d_i\mu_\alpha \cos \delta \sin \alpha - 4.74d_i\mu_\delta \sin \delta \cos \alpha + V_r \cos \delta \cos \alpha, \quad (4)$$

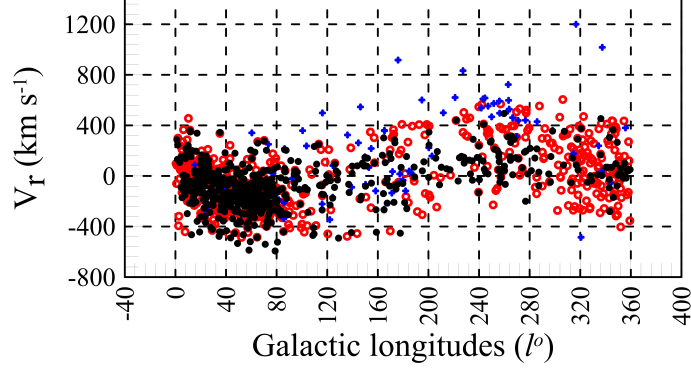


Figure 2. Distribution of (V_r ; km s^{-1}) for three Program HiVels as a function of their galactic longitudes (l°). Program I: black closed circles (591 stars), Program II: blue closed pluses (87 stars), and Program III: red open circles (519 stars).

$$V_y = +4.74d_i\mu_\alpha \cos \delta \cos \alpha - 4.74d_i\mu_\delta \sin \delta \sin \alpha + V_r \cos \delta \sin \alpha, \quad (5)$$

$$V_z = +4.74d_i\mu_\delta \cos \delta + V_r \sin \delta. \quad (6)$$

In what follows, we estimate the velocities dispersion (σ_1 , σ_2 , and σ_3 ; km s^{-1}) using the following equations to specify VEPs as described in the literature (Elsanhoury, 2024; Elsanhoury & Al-Johani, 2023):

$$\begin{aligned} \sigma_1 &= \sqrt{2\rho^{\frac{1}{3}} \cos \frac{\phi}{3} - \frac{k_1}{3}}; \\ \sigma_2 &= \sqrt{-\rho^{\frac{1}{3}} \left\{ \cos \frac{\phi}{3} + \sqrt{3} \sin \frac{\phi}{3} \right\} - \frac{k_1}{3}}; \\ \sigma_3 &= \sqrt{-\rho^{\frac{1}{3}} \left\{ \cos \frac{\phi}{3} - \sqrt{3} \sin \frac{\phi}{3} \right\} - \frac{k_1}{3}}. \end{aligned} \quad (7)$$

ρ and ϕ are calculated as:

$$\rho = \sqrt{-q^3}, \quad (8)$$

$$x = \rho^2 - r^2, \quad (9)$$

$$\phi = \tan^{-1} \left(\frac{\sqrt{x}}{r} \right). \quad (10)$$

The parameters q and r are given by the equations:

$$q = \frac{1}{3}k_2 - \frac{1}{9}k_1^2 \quad ; \quad r = \frac{1}{6}(k_1k_2 - 3k_3) - \frac{1}{27}k_1^3 \quad (11)$$

The coefficients k_1 , k_2 , and k_3 are determined as a function of matrix elements (μ_{ij} ; $\forall i = 1, 2, 3$; $\forall j = 1, 2, 3$):

$$\begin{aligned} k_1 &= -(\mu_{11} + \mu_{22} + \mu_{33}), \\ k_2 &= \mu_{11}\mu_{22} + \mu_{11}\mu_{33} + \mu_{22}\mu_{33} - (\mu_{12}^2 + \mu_{13}^2 + \mu_{23}^2), \\ k_3 &= \mu_{12}^2\mu_{33} + \mu_{13}^2\mu_{22} + \mu_{23}^2\mu_{11} - \mu_{11}\mu_{22}\mu_{33} - 2\mu_{12}\mu_{13}\mu_{23}. \end{aligned} \quad (12)$$

since

$$\begin{aligned} \mu_{11} &= \frac{1}{N} \sum_{i=1}^N U_i^2 - (\bar{U})^2; & \mu_{12} &= \frac{1}{N} \sum_{i=1}^N U_i V_i - \bar{U} \bar{V}; \\ \mu_{13} &= \frac{1}{N} \sum_{i=1}^N U_i W_i - \bar{U} \bar{W}; & \mu_{22} &= \frac{1}{N} \sum_{i=1}^N V_i^2 - (\bar{V})^2; \\ \mu_{23} &= \frac{1}{N} \sum_{i=1}^N V_i W_i - \bar{V} \bar{W}; & \mu_{33} &= \frac{1}{N} \sum_{i=1}^N W_i^2 - (\bar{W})^2. \end{aligned} \quad (13)$$

The direction cosines (l_j, m_j, n_j ; $\forall j = 1, 2, 3$) for the eigenvalue problem (λ_j), matrix elements (μ_{ij}), and velocities dispersion (σ_j) [i.e., $\lambda_j = \sigma_j^2$; $\forall j = 1, 2, 3$] where ($\lambda_1 > \lambda_2 > \lambda_3$), along three axes (Elsanhoury et al., 2015), are mathematically given as follows:

$$l_j = [\mu_{22}\mu_{33} - \sigma_j^2(\mu_{22} + \mu_{33} - \sigma_j^2) - \mu_{23}^2] / D_j, \quad (14)$$

$$m_j = [\mu_{23}\mu_{13} - \mu_{12}\mu_{33} + \sigma_j^2\mu_{12}] / D_j, \quad (15)$$

$$n_j = [\mu_{12}\mu_{23} - \mu_{13}\mu_{22} + \sigma_j^2\mu_{13}] / D_j. \quad (16)$$

and

$$\begin{aligned} D_j^2 &= (\mu_{22}\mu_{33} - \mu_{23}^2)^2 + (\mu_{23}\mu_{13} - \mu_{12}\mu_{33})^2 \\ &+ (\mu_{12}\mu_{23} - \mu_{13}\mu_{22})^2 + 2[(\mu_{22} + \mu_{33})(\mu_{23}^2 - \mu_{22}\mu_{33}) \\ &+ \mu_{12}(\mu_{23}\mu_{13} - \mu_{12}\mu_{33}) + \mu_{13}(\mu_{12}\mu_{23} - \mu_{13}\mu_{22})] \sigma_j^2 \\ &+ (\mu_{33}^2 + 4\mu_{22}\mu_{33} + \mu_{22}^2 - 2\mu_{23}^2 + \mu_{12}^2 + \mu_{13}^2) \sigma_j^4 \\ &- 2(\mu_{22} + \mu_{33}) \sigma_j^6 + \sigma_j^8. \end{aligned}$$

where ($l_j^2 + m_j^2 + n_j^2 = 1$) is an initial test for our code and (l_2) is known as vertex longitude (Mihalas et al., 1983; Elsanhoury, 2016).

3.2. Galactic longitude and latitude parameters

Let L_j and B_j , ($\forall j = 1, 2, 3$) be the galactic longitude and latitude of the directions, respectively, which correspond to the extreme values of the dispersion, then

$$L_j = \tan^{-1}\left(\frac{-m_j}{l_j}\right), \quad (17)$$

$$B_j = \sin^{-1}(n_j). \quad (18)$$

3.3. Fundamental solar elements

For Program stars having a space velocities $(\bar{U}, \bar{V}, \bar{W})$, the components of the Sun's velocities are referred to as $(U_\odot, V_\odot, \text{ and } W_\odot)$, where $(U_\odot = -\bar{U})$, $(V_\odot = -\bar{V})$, and $(W_\odot = -\bar{W})$. Therefore, the solar elements (S_\odot, l_A, b_A) with spatial velocity considered may take the following:

$$S_\odot = \sqrt{\bar{U}^2 + \bar{V}^2 + \bar{W}^2}, \quad (19)$$

$$l_A = \tan^{-1} \left(\frac{-\bar{V}}{\bar{U}} \right), \quad (20)$$

$$b_A = \sin^{-1} \left(\frac{-\bar{W}}{S_\odot} \right). \quad (21)$$

In what follows, we estimate the Sun's local velocity from radial velocities, by letting $X_\odot^\bullet, Y_\odot^\bullet$ and Z_\odot^\bullet be the components of the Sun's velocity relative to x, y , and z axes with the origin at the observer. Therefore, $X_\odot^\bullet = -\bar{V}_x$, $Y_\odot^\bullet = -\bar{V}_y$, and $Z_\odot^\bullet = -\bar{V}_z$. From there, we can find the apex of the Sun's way from formulae,

$$\alpha_A = \tan^{-1} \left(\frac{Y_\odot^\bullet}{X_\odot^\bullet} \right), \quad (22)$$

$$\delta_A = \tan^{-1} \left(\frac{Z_\odot^\bullet}{\sqrt{(X_\odot^\bullet)^2 + (Y_\odot^\bullet)^2}} \right). \quad (23)$$

and the Sun's velocity is given by

$$S_\odot = \sqrt{(X_\odot^\bullet)^2 + (Y_\odot^\bullet)^2 + (Z_\odot^\bullet)^2}, \quad (24)$$

Where S_\odot denotes the absolute value of the Sun's velocity relative to the three Program stars under consideration, (l_A, b_A) are galactic longitude and galactic latitude of the solar apex, respectively, and (α_A, δ_A) is the galactic right ascension and declination with respective manner of the solar apex. Figure 3, shows the HiVels in three projection velocities (i.e., U, V , and W) with respect to the galactic center. This allows researchers to examine stellar populations in the circumsolar area of the Galaxy. Of great interest is the UV plane, where all stars can be properly classified into multiple families. Nearby stars mostly originate from the disk, which has a distinctive velocity dispersion $\sim -500 \text{ km s}^{-1}$ along each coordinate.

following the computational algorithm developed by [Elsanhoury et al. \(2015\)](#) to serve and compute the VEPs and the convergent point (CP) of three HiVels Programs, including various kinematic parameters (e.g., spatial velocities, velocities dispersion, direction cosines, solar elements, ... etc.) and the ratios of

(σ_2/σ_1) and (σ_3/σ_1) , into which the obtained results of these ratios ranged from 0.75 to 0.86 & 0.40 to 0.60, respectively.

Stars in the galactic disk have the largest velocity dispersion in the radial direction, which is why it is said that the velocity ellipsoid's longest axis points approximately in the direction of the galactic center. The velocity ellipsoid's longest axis points roughly in the direction of the galactic center because one of its axes is oriented normally to the plane of the galaxy, allowing the other two axes to also lie there. The angle between a group of stars' average V_r vector and the line connecting the Sun to the galactic center is known as the vertex deviation or longitude of the vertex (l_2). The kinematic characteristics of the studied star population (e.g., HiVels) can be examined in this way. In the MW's thin disk, the velocity ellipsoid is oriented almost along the radial direction (toward the galactic center) because the vertex's longitude is usually near 0° (Elsanhoury et al., 2015; Elsanhoury, 2016; Bisht et al., 2020; Mihalas & Binney, 1981). The original numerical results are listed in Table 2 and Table 3, including the solar elements.

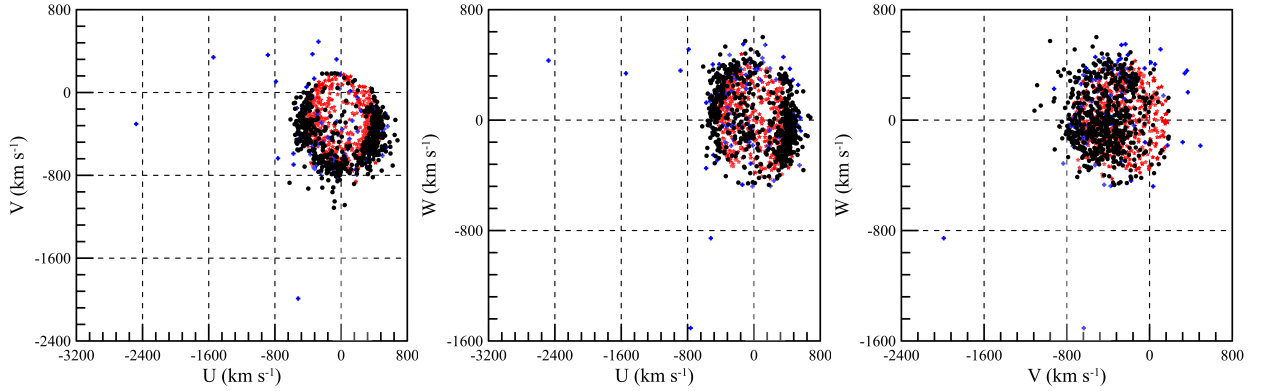


Figure 3. Velocity components distributions UV , UW , and VW relative to the Galaxy center of three Program HiVels calculated by us. Program I: black closed circles – 591 HiVels, Program II: blue closed pluses – 87 HiVels, and Program III: red open circles – 519 stars.

3.4. Convergent Point (CP)

Usually, stars in a stellar association and/or moving group have a common chemical composition, space velocity, age, and distance which indicates that they are moving across the Galaxy together. The apparent movement of these stars as viewed by the observer, however, varies slightly based on their position in the MW. Their PM vectors indicate the velocity and bearing of the stars'

passage across the MW. Typically, in stellar kinematics, the coherent point in the direction of one location on the celestial sphere is well-defined as a vertex, apex, or CP with equatorial coordinates (A_o, D_o) . Several techniques are stated for this purpose like i) the classical CP method (Boss, 1908), ii) the individual star apex (AD-diagram), known and developed by Chupina et al. (2001, 2006), and iii) the convergent point search method (CPSM) edited by Galli et al. (2012). In present analysis, we specifically focus on the AD chart method, which relies on the distribution of individual apexes within the equatorial coordinate system and was employed (Bisht et al., 2020; Elsanhoury, 2021; Maurya et al., 2021). Eqs. 4, 5, and 6 of average space velocity vectors are used in this manner to get the equatorial coordinates of the (A_o, D_o) in the following formulae. The obtained results are listed in the last row of Table 2.

$$\begin{aligned} A_o &= \tan^{-1} \left(\frac{\overline{V}_y}{\overline{V}_x} \right) \\ \& \quad D_o &= \tan^{-1} \left(\frac{\overline{V}_z}{\sqrt{\overline{V}_x^2 + \overline{V}_y^2}} \right) \end{aligned} \quad (25)$$

4. Galactic rotation constants

The stars offer a perfect sample for understanding the composition and development of the galactic disk and determining the MW constant parameters. These constants are crucial for understanding how stars, gas, and other objects move within the Galaxy's gravitational potential. Moreover, describes the rotation curve and the motion of objects relative to the galactic center. The differential rotation and local angular velocity (i.e., local rotational features) of the MW Galaxy are described by two fundamental parameters, A and B (i.e., Oort's constants (Oort, 1927a)). They give the dynamic structure of the MW, including its rotation curve and the distribution of matter within it. In addition to helping quantify the shear and turbulent flow of the rotation of the Galaxy, these constants are used to examine how the velocity of stars varies with their distance from the galactic center. According to Oort (Oort, 1927a,b), the constants (A & B) were then calculated using V_r and PM , yielding the values $A \approx 19 \text{ km s}^{-1} \text{ kpc}^{-1}$ and $B \approx -24 \text{ km s}^{-1} \text{ kpc}^{-1}$. In his study, the relatively smooth rotating curve of the Galaxy was demonstrated, cutting out the hypothesis that it rotates like a rigid body.

Following this, numerous attempts have been made using different tracers to calculate the Oort constants and illustrate the galactic rotation. After reviewing the earlier data, Kerr & Lynden-Bell (1986) came to the following conclusions: $A = 14.40 \pm 1.20 \text{ km s}^{-1} \text{ kpc}^{-1}$ and $B = -12.00 \pm 2.80 \text{ km s}^{-1} \text{ kpc}^{-1}$. To determine that $A = -14.82 \pm 0.84 \text{ km s}^{-1} \text{ kpc}^{-1}$ and $B = -12.37 \pm 0.64$

Table 2. VEPs and CPs of the three Program HiVels calculated by us.

Parameters	Program I: 591 HiVels ($0.10 \leq d(\text{kpc}) \leq 15.40$)
$\overline{V_x}, \overline{V_y}, \overline{V_z}$ (km s ⁻¹)	-218.43 ± 14.76, 139.79 ± 11.83, -343.81 ± 18.54
$\overline{U}, \overline{V}, \overline{W}$ (km s ⁻¹)	56.61 ± 7.52, -426.79 ± 20.66, 9.88 ± 3.14
$\lambda_1, \lambda_2, \lambda_3$ (km s ⁻¹)	239234, 137669, 38478.70
$\sigma_1, \sigma_2, \sigma_3$ (km s ⁻¹)	489.12 ± 22.12, 371.04 ± 19.26, 196.16 ± 14.01
$\overline{\sigma}_O$ (km s ⁻¹)	644.50 ± 15.40
$(l_1, m_1, n_1)^o$	0.2869 ± 0.002, -0.9578 ± 0.002, -0.0220 ± 0.001
$(l_2, m_2, n_2)^o$	-0.9145 ± 0.003, -0.2806 ± 0.002, 0.2916 ± 0.002
$(l_3, m_3, n_3)^o$	0.2854 ± 0.002, 0.0636 ± 0.001, 0.9563 ± 0.002
$L_j, j = 1, 2, 3$	73.33, 162.94, 167.45
$B_j, j = 1, 2, 3$	-1.26, 16.95, 73.00
S_{\odot} (km s ⁻¹)	430.641 ± 20.75
$(l_A, b_A)^o$	82.44 ± 0.11, -1.32 ± 0.02
$(\alpha_A, \delta_A)^o$	-32.62 ± 0.17, -52.97 ± 0.86
$(A_O, D_O)^o$	147.382 ± 0.08, -52.973 ± 0.14
Parameters	Program II: 87 HiVels ($0.30 \leq d(\text{kpc}) \leq 108.64$)
$\overline{V_x}, \overline{V_y}, \overline{V_z}$ (km s ⁻¹)	-256.92 ± 16.03, 276.45 ± 16.63, -232.17 ± 15.24
$\overline{U}, \overline{V}, \overline{W}$ (km s ⁻¹)	114.88 ± 10.72, -422.77 ± 20.56, 66.39 ± 8.15
$\lambda_1, \lambda_2, \lambda_3$ (km s ⁻¹)	309649, 226100, 108921
$\sigma_1, \sigma_2, \sigma_3$ (km s ⁻¹)	556.46 ± 23.59, 475.50 ± 21.81, 330.03 ± 18.17
$\overline{\sigma}_O$ (km s ⁻¹)	802.92 ± 28.34
$(l_1, m_1, n_1)^o$	0.2759 ± 0.002, 0.9610 ± 0.002, 0.0181 ± 0.001
$(l_2, m_2, n_2)^o$	-0.9528 ± 0.003, 0.2710 ± 0.002, 0.1368 ± 0.001
$(l_3, m_3, n_3)^o$	0.1265 ± 0.001, -0.0550 ± 0.001, 0.9904 ± 0.002
$L_j, j = 1, 2, 3$	-73.98, -164.13, -156.51
$B_j, j = 1, 2, 3$	1.04, 7.86, 82.07
S_{\odot} (km s ⁻¹)	443.100 ± 21.05
$(l_A, b_A)^o$	-74.80 ± 0.12, -8.62 ± 0.34
$(\alpha_A, \delta_A)^o$	-47.10 ± 0.15, -31.60 ± 0.18
$(A_O, D_O)^o$	132.902 ± 0.09, -31.600 ± 0.18
Parameters	Program III: 519 HiVels ($0.29 \leq d(\text{kpc}) \leq 16.44$)
$\overline{V_x}, \overline{V_y}, \overline{V_z}$ (km s ⁻¹)	-157.41 ± 12.55, 121.11 ± 11.00, -230.11 ± 15.17
$\overline{U}, \overline{V}, \overline{W}$ (km s ⁻¹)	14.46 ± 3.80, -303.43 ± 17.42, 10.98 ± 3.31
$\lambda_1, \lambda_2, \lambda_3$ (km s ⁻¹)	143180, 80747.10, 34595.50
$\sigma_1, \sigma_2, \sigma_3$ (km s ⁻¹)	378.39 ± 19.45, 284.16 ± 16.86, 186.00 ± 13.64
$\overline{\sigma}_O$ (km s ⁻¹)	508.45 ± 22.55
$(l_1, m_1, n_1)^o$	0.1307 ± 0.001, -0.9910 ± 0.002, -0.0275 ± 0.002
$(l_2, m_2, n_2)^o$	-0.9403 ± 0.003, -0.1327 ± 0.001, 0.3134 ± 0.003
$(l_3, m_3, n_3)^o$	0.3142 ± 0.003, 0.0151 ± 0.001, 0.0950 ± 0.002
$L_j, j = 1, 2, 3$	82.49, 171.97, 177.24
$B_j, j = 1, 2, 3$	-1.57, 18.27, 71.67
S_{\odot} (km s ⁻¹)	303.977 ± 17.43
$(l_A, b_A)^o$	87.27 ± 0.11, -2.07 ± 0.03
$(\alpha_A, \delta_A)^o$	-37.57 ± 0.16, -49.20 ± 0.14
$(A_O, D_O)^o$	142.43 ± 0.08, -49.21 ± 0.14

km s⁻¹ kpc⁻¹, [Feast & Whitelock \(1997\)](#) adopted 220 galactic Cepheids with Hipparcos *PM*. Considering $R_o = 7.66 \pm 0.32$ kpc by [Metzger et al. \(1998\)](#), therefore, the obtained comparable outcome for $A = 15.50 \pm 0.40$ km s⁻¹ kpc⁻¹ using Cepheids. Recently, [Nouh & Elsanhoury \(2020\)](#) obtained a comparable outcome of A & B with 15.60 ± 1.60 & -13.90 ± 1.80 km s⁻¹ kpc⁻¹, [Elsanhoury et al. \(2021\)](#) computed Oort constants like $A = 14.69 \pm 0.61$ km s⁻¹ kpc⁻¹ and $B = -16.70 \pm 0.67$ km s⁻¹ kpc⁻¹, and [Elsanhoury \(2024\)](#) have $A = 12.91 \pm 0.16$ km s⁻¹ kpc⁻¹ and $B = -13.16 \pm 0.27$ km s⁻¹ kpc⁻¹.

Here, we calculate the Oort constants (A & B) considered for three-Program HiVels using the LAMOST and DR3 archives. With an amplitude that rises linearly with distance, we follow the discovery that the heliocentric V_r shows a double sine-wave variation with galactic longitude ([Balona & Feast,](#)

Table 3. Ratios of velocity dispersions and the solar velocities for our three program HiVels and other components of the disks with different authors.

Type	S_{\odot} (km s ⁻¹)	σ_2/σ_1	σ_3/σ_1	References
Program I – 591 stars	430.641 ± 20.75	0.76	0.40	Current Study
Program II – 87 stars	443.100 ± 21.05	0.86	0.60	Current Study
Program III – 591 stars	303.977 ± 17.43	0.75	0.49	Current Study
Inner halo ($d \leq 15$ kpc)	213.36 ± 14.61	0.70	0.52	Nouh & Elsanhoury (2020)
Outer halo ($d = 15 - 20$ kpc)	210.14 ± 14.50	0.76	0.61	Nouh & Elsanhoury (2020)
Halo disk	-	0.56	0.56	Yan et al. (2020)
Thin disk	-	0.57	0.46	Yan et al. (2020)
Thick disk	-	0.57	0.52	Yan et al. (2020)
Thin disk	-	0.62	0.62	Soubiran et al. (2003)
Thick disk	-	0.51	0.51	Soubiran et al. (2003)
$8.9 \geq M_V \geq 8.0$	-	0.72 ± 0.04	0.62 ± 0.04	Dyer (1956)
$M_V \geq 9.0$	-	0.67 ± 0.05	0.56 ± 0.04	Dyer (1956)

1974).

$$V_r = -2A(R_{gc} - R_o) \sin l \cos b + K, \quad (26)$$

where (K ; km s⁻¹) is a correction term that can be understood as systematic motions of massive stellar groups, systematic inaccuracies in the V_r caused by motions within stellar atmospheres, gravitational redshift, and erroneous wavelength combinations (Feast & Shuttlesworth, 1965), where l and b stand for the specific star’s longitude and latitude, respectively, $R_o = 8.20 \pm 0.10$ kpc (Bland-Hawthorn et al., 2019) is the distance from the Sun to the galactic center, and R_{gc} is the star’s radial distance from the galactic center, is the cylindrical radius vector, and it is determined by

$$R_{gc}^2 = R_o^2 + d^2 - 2R_o d \cos l. \quad (27)$$

Table 4 lists our three HiVels Investigations for which we computed the Oort constants A and B . Column 3’s least-squares fit of Eq. 26 yields the first Oort constant (A ; km s⁻¹ kpc⁻¹), while the fourth column’s is the second Oort constant (B ; km s⁻¹ kpc⁻¹) calculated using the relation $(\sigma_2/\sigma_1)^2 = -B/(A - B)$ (Bisht et al., 2020). The ratio (σ_2/σ_1) is calculated using the computational method covered in Section 3. The angular velocity is shown in column 5 ($|A - B|$; km s⁻¹ kpc⁻¹), and the rotational velocity V_o calculated using the well-known relation $V_o = |A - B| R_o$, where $R_o = 8.20 \pm 0.10$ kpc and is stated in the last column. Our mean Oort and rotational constants as compared with previous researchers are presented in Table 5, it’s clear that Oort constants and galactic rotational parameters were computed for about 304,267 main sequence

Table 4. Velocity dispersion and rotation constants for three program HiVels under study.

Program HiVels	σ_2/σ_1	A km s ⁻¹ kpc ⁻¹	B km s ⁻¹ kpc ⁻¹	$ A - B $ km s ⁻¹ kpc ⁻¹	V_o km s ⁻¹
I ($0.10 \leq d(\text{kpc}) \leq 15.40$); 591 stars	0.76	15.427 ± 0.25	-21.095 ± 0.22	36.522 ± 6.04	299.48 ± 17.31
II ($0.30 \leq d(\text{kpc}) \leq 108.64$); 87 stars	0.86	3.883 ± 0.51	-11.029 ± 0.30	14.912 ± 3.86	122.28 ± 11.06
III ($0.29 \leq d(\text{kpc}) \leq 16.44$); 519 stars	0.75	16.510 ± 0.25	-21.227 ± 0.22	37.737 ± 6.14	309.44 ± 17.59

Table 5. Velocity dispersion and rotation constants for three program HiVels under study.

A km s ⁻¹ kpc ⁻¹	B km s ⁻¹ kpc ⁻¹	$ A - B $ km s ⁻¹ kpc ⁻¹	Methods V_r/PMs	References
11.94 ± 0.29	-17.78 ± 0.24	25.07 ± 5.01	V_r	Current Study
15.30 ± 0.40	-11.90 ± 0.40	27.20	PMs	Bovy (2017)
15.10 ± 0.10	-13.40 ± 0.40	28.40	PMs	Li et al. (2019)
15.73 ± 0.32	-12.67 ± 0.34	28.40	PMs	Krisanova et al. (2020)
15.60 ± 1.60	-13.90 ± 1.80	29.50 ± 0.20	V_r	Nouh & Elsanhoury (2020)
16.31 ± 0.89	-11.99 ± 0.79	28.30	PMs	Wang et al. (2021)
14.69 ± 0.61	-16.70 ± 0.67	31.39	V_r	Elsanhoury et al. (2021)
15.60 ± 1.60	-15.80 ± 1.70	31.40 ± 2.30	V_r	Guo & Qi (2023)
12.91 ± 0.16	-13.16 ± 0.27	26.06	V_r	Elsanhoury & Al-Johani (2023)

stars from the Gaia DR1 using data at a typical heliocentric distance of 230 pc ([Bovy, 2017](#)), a sample of stars within 500 parsecs used the Gaia DR2 data ([Li et al., 2019](#)), using the trigonometric parallaxes and PMs of over 25,000 young stars from the Gaia DR2 dataset ([Krisanova et al., 2020](#)), using a sample of halo red giants and the radial and spatial velocities of 1,583 red giant stars collected from the SEGUE-1 and SEGUE-2 surveys ([Nouh & Elsanhoury, 2020](#)), sample of 5,627 A -type stars selected from the LAMOST surveys that were located within 0.60 kpc ([Wang et al., 2021](#)), devoted mid to late M -type stars ([Elsanhoury et al., 2021](#)), for a clean sample of stars (130,665) within 100 pc ([Guo & Qi, 2023](#)) computed these constants with a maximum likelihood model by using the Gaia Catalog of Nearby Stars (GCNS) ([Gaia Collaboration et al., 2021](#)), and for high and low galactic latitudes of K dwarfs ([Elsanhoury & Al-Johani, 2023](#)).

5. Discussion and conclusion

The velocity distribution (U, V, W) of stars in three spatial directions ($\sigma_1, \sigma_2, \sigma_3$) is known as the velocity ellipsoid in galactic kinematics. The ellipsoid's shape

reflects the anisotropy in the star motion, and its primary axes relate to the directions with the largest and smallest velocity dispersion. Velocity ellipsoids vary among star populations. For instance, thick disk and halo stars exhibit more isotropic ellipsoids and bigger velocity dispersions than thin disk stars, which have comparatively small dispersions. In this study, we calculated the kinematical parameters, convergent point, and the Oort constants A and B of three Programs (i.e., 591, 87, and 519 stars) of high velocity stars located ($0.10 \geq d(\text{kpc}) \geq 109$). The following summarizes the main findings of the current studies:

- We retrieved high velocities in both mean spatial velocities (U , V , W , and V_{space} ; km s^{-1}), Program I (56.61 ± 7.52 , -426.79 ± 20.66 , 9.88 ± 3.14 , and 430.641 ± 20.75), Program II (114.88 ± 10.72 , -422.77 ± 20.56 , 66.39 ± 8.15 , and 443.100 ± 21.05), and Program III (14.46 ± 3.80 , -303.43 ± 17.42 , 10.98 ± 3.31 , and 303.977 ± 17.43) and the mean velocity dispersion (σ_1 , σ_2 , σ_3 , and σ_o ; km s^{-1}), Program I (489.12 ± 22.12 , 371.04 ± 19.26 , 196.16 ± 14.01 , and 644.50 ± 15.40), Program II (556.46 ± 23.59 , 475.50 ± 21.81 , 330.03 ± 18.17 , and 802.92 ± 28.34), and Program III (378.39 ± 19.45 , 284.16 ± 16.86 , 186.00 ± 13.64 , and 508.45 ± 22.55).
- Our obtained results of the l_2 are: $-0^\circ.9145 \pm 0^\circ.003$ (Program I), $-0^\circ.9528 \pm 0^\circ.003$ (Program II), and $-0.9403 \pm 0^\circ.003$ (Program III), this obtained results are in line with that of [Mihalas & Binney \(1981\)](#) and many authors, e.g., $l_2 = -0^\circ.3454$, $-0^\circ.6735$, and $-0^\circ.0264$ ([Elsanhoury, 2024](#)) and $-0^\circ.87$ & $-0^\circ.91$ ([Elsanhoury et al., 2018](#)).
- We have determined the convergent points (A_o , D_o), Program I: $147^\circ.382 \pm 0^\circ.08$, $-52^\circ.973 \pm 0^\circ.14$, Program II: $132^\circ.902 \pm 0^\circ.09$, $-31^\circ.600 \pm 0^\circ.18$, and Program III: $142^\circ.43 \pm 0^\circ.08$, $-49^\circ.21 \pm 0^\circ.14$.
- The mean values of the Oort's constants, $A = 11.94 \pm 0.29$ and $B = -17.78 \pm 0.24 \text{ km s}^{-1} \text{ kpc}^{-1}$ as listed in Table 5. Therefore, the mean angular velocity $|A - B| = 25.07 \pm 5.01 \text{ km s}^{-1} \text{ kpc}^{-1}$ and the rotational velocity $V_o = 243.72 \pm 15.61 \text{ km s}^{-1}$.
- In regions where stars are to be expected to be quite a way distant on average like our consideration of HiVels. The measured values of A and B may contain significant inaccuracies due to both long distances ([Lewis, 1990](#)) and the choice of kinematic model (V_r or PM) ([Hanson, 1987](#)) as Table 4 makes clear with Program II. [Lewis \(1990\)](#) reported that this is due to two effects. First, the proper motion along declination μ_δ nearly equal to the ratio of (V_y/d) , i.e., $\mu_\delta \sim (V_y/d)$ and $A \sim \mu_\delta$, thus if d increases, the value of A will decrease, as clearly seen in Program II of Table 4. But V_y also dependent on $(\cos \alpha)$ and is dependent on distance d (see Eq. 5). Therefore, these two effects should affect both A and B in a roughly equal manner ([Lewis, 1990](#)).

Acknowledgements. We sincerely thank the anonymous referee for their valuable suggestions, which have significantly improved the quality of this paper. This work presents results from the European Space Agency space mission Gaia. Gaia

data are being processed by the Gaia Data Processing and Analysis Consortium (DPAC). Funding for the DPAC is provided by national institutions, in particular, the institutions participating in the Gaia MultiLateral Agreement (MLA). The Gaia mission website is <https://www.cosmos.esa.int/gaia>. The Gaia archive website is <https://archives.esac.esa.int/gaia>. The author extend their appreciation to the Deanship of Scientific Research at Northern Border University, Arar, KSA for funding this research work through the project number "NBU-FFR-2025-237-03".

Guoshoujing Telescope (Large Sky Area Multi-Object Fiber Spectroscopic Telescope LAMOST) is a National Major Scientific Project built by the Chinese Academy of Sciences. Funding for the project has been provided by the National Development and Reform Commission. LAMOST is operated and managed by the National Astronomical Observatories, Chinese Academy of Sciences.

Data availability: We have used the different data sets for high velocity stars, which are publicly available at the following links:

- <https://vizier.cds.unistra.fr/viz-bin/VizieR?-source=J/ApJS/252/3>
- <https://vizier.cds.unistra.fr/viz-bin/VizieR?-source=J/AJ/166/12>
- <https://vizier.cds.unistra.fr/viz-bin/VizieR?-source=J/AJ/167/76>
- https://vizier.cds.unistra.fr/viz-bin/VizieR-3?-source=I/355/gaiadr3&-out.max=50&-out.form=HTML%20Table&-out.add=_r&-out.add=_RAJ,_DEJ&-sort=_r&-oc.form=sexa

References

- Abadi, M. G., Navarro, J. F., & Steinmetz, M., An Alternative Origin for Hypervelocity Stars. 2009, *Astrophysical Journal, Letters*, **691**, L63, DOI:10.1088/0004-637X/691/2/L63
- Alam, S., Albareti, F. D., Allende Prieto, C., et al., The Eleventh and Twelfth Data Releases of the Sloan Digital Sky Survey: Final Data from SDSS-III. 2015, *Astrophysical Journal, Supplement*, **219**, 12, DOI:10.1088/0067-0049/219/1/12
- Balona, L. A. & Feast, M. W., A new determination from OB stars of the galactic rotation constants and the distance to the galactic centre. 1974, *Monthly Notices of the RAS*, **167**, 621, DOI:10.1093/mnras/167.3.621
- Bauer, E. B., White, C. J., & Bildsten, L., Remnants of Subdwarf Helium Donor Stars Ejected from Close Binaries with Thermonuclear Supernovae. 2019, *Astrophysical Journal*, **887**, 68, DOI:10.3847/1538-4357/ab4ea4
- Bisht, D., Elsanhoury, W. H., Zhu, Q., et al., An Investigation of Poorly Studied Open Cluster NGC 4337 Using Multicolor Photometric and Gaia DR2 Astrometric Data. 2020, *Astronomical Journal*, **160**, 119, DOI:10.3847/1538-3881/ab9ffd
- Blaauw, A., On the origin of the O- and B-type stars with high velocities (the “run-away” stars), and some related problems. 1961, *Bulletin Astronomical Institute of the Netherlands*, **15**, 265
- Bland-Hawthorn, J., Sharma, S., Tepper-Garcia, T., et al., The GALAH survey and Gaia DR2: dissecting the stellar disc’s phase space by age, action, chemistry, and location. 2019, *Monthly Notices of the RAS*, **486**, 1167, DOI:10.1093/mnras/stz217

- Boss, L. J., Convergent of a moving cluster in Taurus. 1908, *Astronomical Journal*, **26**, 31, DOI:10.1086/103802
- Bovy, J., Galactic rotation in Gaia DR1. 2017, *Monthly Notices of the RAS*, **468**, L63, DOI:10.1093/mnras1/s1x027
- Bovy, J., Allende Prieto, C., Beers, T. C., et al., The Milky Way's Circular-velocity Curve between 4 and 14 kpc from APOGEE data. 2012, *Astrophysical Journal*, **759**, 131, DOI:10.1088/0004-637X/759/2/131
- Bromley, B. C., Kenyon, S. J., Geller, M. J., et al., Hypervelocity Stars: Predicting the Spectrum of Ejection Velocities. 2006, *Astrophysical Journal*, **653**, 1194, DOI:10.1086/508419
- Buder, S., Sharma, S., Kos, J., et al., The GALAH+ survey: Third data release. 2021, *Monthly Notices of the RAS*, **506**, 150, DOI:10.1093/mnras/stab1242
- Capuzzo-Dolcetta, R. & Fragione, G., High-velocity stars from close interaction of a globular cluster and a supermassive black hole. 2015, *Monthly Notices of the RAS*, **454**, 2677, DOI:10.1093/mnras/stv2123
- Chupina, N. V., Reva, V. G., & Vereshchagin, S. V., The geometry of stellar motions in the nucleus region of the Ursa Major kinematic group. 2001, *Astronomy and Astrophysics*, **371**, 115, DOI:10.1051/0004-6361:20010337
- Chupina, N. V., Reva, V. G., & Vereshchagin, S. V., Kinematic structure of the corona of the Ursa Major flow found using proper motions and radial velocities of single stars. 2006, *Astronomy and Astrophysics*, **451**, 909, DOI:10.1051/0004-6361:20054009
- Contigiani, O., Rossi, E. M., & Marchetti, T., On measuring the Galactic dark matter halo with hypervelocity stars. 2019, *Monthly Notices of the RAS*, **487**, 4025, DOI:10.1093/mnras/stz1547
- Cui, X.-Q., Zhao, Y.-H., Chu, Y.-Q., et al., The Large Sky Area Multi-Object Fiber Spectroscopic Telescope (LAMOST). 2012, *Research in Astronomy and Astrophysics*, **12**, 1197, DOI:10.1088/1674-4527/12/9/003
- De Silva, G. M., Freeman, K. C., Bland-Hawthorn, J., et al., The GALAH survey: scientific motivation. 2015, *Monthly Notices of the RAS*, **449**, 2604, DOI:10.1093/mnras/stv327
- Dyer, Jr., E. R., An analysis of the space motions of red dwarf stars. 1956, *Astronomical Journal*, **61**, 228, DOI:10.1086/107332
- Eilers, A.-C., Hogg, D. W., Rix, H.-W., & Ness, M. K., The Circular Velocity Curve of the Milky Way from 5 to 25 kpc. 2019, *Astrophysical Journal*, **871**, 120, DOI:10.3847/1538-4357/aaf648
- Elsanhoury, W. H., Kinematics and Velocity Ellipsoid Parameters of Stellar Groups and Open Star Clusters: II Cool Stars. 2016, *Astrophysics*, **59**, 246, DOI:10.1007/s10511-016-9430-0
- Elsanhoury, W. H., Photometric and kinematical analysis of Kopusov 12 and Kopusov 43 open clusters. 2021, *Journal of Astrophysics and Astronomy*, **42**, 90, DOI:10.1007/s12036-021-09771-x

- Elsanhoury, W. H., Kinematical and ellipsoidal properties of the inner-halo hot subdwarfs observed in Gaia DR3 and LAMOST DR7. 2024, *New Astronomy*, **112**, 102258, DOI:10.1016/j.newast.2024.102258
- Elsanhoury, W. H. & Al-Johani, A. S., Kinematical and ellipsoidal properties of K dwarfs in the solar neighborhood of the Gaia era. 2023, *Astronomische Nachrichten*, **344**, e20230047, DOI:10.1002/asna.20230047
- Elsanhoury, W. H., Nouh, M. I., & Abdel-Rahman, H. I., Kinematics and Velocity Ellipsoid of the Solar Neighborhood White Dwarfs. 2015, *Revista Mexicana de Astronomia y Astrofisica*, **51**, 199, DOI:10.48550/arXiv.1503.03595
- Elsanhoury, W. H., Nouh, M. I., Branham, R. L., & Al-Johani, A. S., Kinematics and ellipsoidal motion of the mid to late M-type stars. 2021, *Astronomische Nachrichten*, **342**, 989, DOI:10.1002/asna.20210019
- Elsanhoury, W. H., Postnikova, E. S., Chupina, N. V., et al., The Pleiades apex and its kinematical structure. 2018, *Astrophysics and Space Science*, **363**, 58, DOI:10.1007/s10509-018-3268-3
- Feast, M. & Whitelock, P., Galactic kinematics of Cepheids from HIPPARCOS proper motions. 1997, *Monthly Notices of the RAS*, **291**, 683, DOI:10.1093/mnras/291.4.683
- Feast, M. W. & Shuttleworth, M., The kinematics of B stars, cepheids, galactic clusters and interstellar gas in the Galaxy. 1965, *Monthly Notices of the RAS*, **130**, 243, DOI:10.1093/mnras/130.4.245
- Feltzing, S., Zhao, G., Walton, N. A., & Whitelock, P., eds. 2014, IAU Symposium, Vol. **298**, *Setting the scene for Gaia and LAMOST*
- Gaia Collaboration, Prusti, T., de Bruijne, J. H. J., et al., The Gaia mission. 2016, *Astronomy and Astrophysics*, **595**, A1, DOI:10.1051/0004-6361/201629272
- Gaia Collaboration, Smart, R. L., Sarro, L. M., et al., Gaia Early Data Release 3. The Gaia Catalogue of Nearby Stars. 2021, *Astronomy and Astrophysics*, **649**, A6, DOI:10.1051/0004-6361/202039498
- Gaia Collaboration, Vallenari, A., Brown, A. G. A., et al., Gaia Data Release 3. Summary of the content and survey properties. 2023, *Astronomy and Astrophysics*, **674**, A1, DOI:10.1051/0004-6361/202243940
- Galli, P. A. B., Teixeira, R., Ducourant, C., Bertout, C., & Benevides-Soares, P., A new method for calculating the convergent point of a moving group. 2012, *Astronomy and Astrophysics*, **538**, A23, DOI:10.1051/0004-6361/201118277
- Gnedin, O. Y., Gould, A., Miralda-Escudé, J., & Zentner, A. R., Probing the Shape of the Galactic Halo with Hypervelocity Stars. 2005, *Astrophysical Journal*, **634**, 344, DOI:10.1086/496958
- Guo, S. & Qi, Z., Oort Constants and Local Stellar Kinematics from GCNS. 2023, *Universe*, **9**, 252, DOI:10.3390/universe9060252
- Gvaramadze, V. V., Gualandris, A., & Portegies Zwart, S., On the origin of high-velocity runaway stars. 2009, *Monthly Notices of the RAS*, **396**, 570, DOI:10.1111/j.1365-2966.2009.14809.x

- Hanson, R. B., Lick Northern Proper Motion Program. II. Solar Motion and Galactic Rotation. 1987, *Astronomical Journal*, **94**, 409, DOI:10.1086/114481
- Hills, J. G., Hyper-velocity and tidal stars from binaries disrupted by a massive Galactic black hole. 1988, *Nature*, **331**, 687, DOI:10.1038/331687a0
- Huang, Y., Liu, X. W., Yuan, H. B., et al., The Milky Way's rotation curve out to 100 kpc and its constraint on the Galactic mass distribution. 2016, *Monthly Notices of the RAS*, **463**, 2623, DOI:10.1093/mnras/stw2096
- Justham, S., Wolf, C., Podsiadlowski, P., & Han, Z., Type Ia supernovae and the formation of single low-mass white dwarfs. 2009, *Astronomy and Astrophysics*, **493**, 1081, DOI:10.1051/0004-6361:200810106
- Kenyon, S. J., Bromley, B. C., Geller, M. J., & Brown, W. R., Hypervelocity Stars: From the Galactic Center to the Halo. 2008, *Astrophysical Journal*, **680**, 312, DOI:10.1086/587738
- Kerr, F. J. & Lynden-Bell, D., Review of galactic constants. 1986, *Monthly Notices of the RAS*, **221**, 1023, DOI:10.1093/mnras/221.4.1023
- Krisanova, O. I., Bobylev, V. V., & Bajkova, A. T., Galactic Rotation Parameters Based on Stars from Active Star-Forming Regions with Data from the Gaia DR2 Catalogue. 2020, *Astronomy Letters*, **46**, 370, DOI:10.1134/S1063773720060067
- Kunder, A., Kordopatis, G., Steinmetz, M., et al., The Radial Velocity Experiment (RAVE): Fifth Data Release. 2017, *Astronomical Journal*, **153**, 75, DOI:10.3847/1538-3881/153/2/75
- Lei, Z., Zhao, J., Németh, P., & Zhao, G., Hot Subdwarf Stars Identified in Gaia DR2 with Spectra of LAMOST DR6 and DR7. I. Single-lined Spectra. 2020, *Astrophysical Journal*, **889**, 117, DOI:10.3847/1538-4357/ab660a
- Leonard, P. J. T., The Maximum Possible Velocity of Dynamically Ejected Runaway Stars. 1991, *Astronomical Journal*, **101**, 562, DOI:10.1086/115704
- Leonard, P. J. T. & Duncan, M. J., Runaway Stars from Young Star Clusters Containing Initial Binaries. II. A Mass Spectrum and a Binary Energy Spectrum. 1990, *Astronomical Journal*, **99**, 608, DOI:10.1086/115354
- Lewis, J. R., Faint stars and Oort's constants. 1990, *Monthly Notices of the RAS*, **244**, 247
- Li, C., Zhao, G., & Yang, C., Galactic Rotation and the Oort Constants in the Solar Vicinity. 2019, *Astrophysical Journal*, **872**, 205, DOI:10.3847/1538-4357/ab0104
- Li, Q.-Z., Huang, Y., Dong, X.-B., et al., On the Origins of Extreme Velocity Stars as Revealed by Large-scale Galactic Surveys. 2023, *Astronomical Journal*, **166**, 12, DOI:10.3847/1538-3881/acd1dc
- Li, Y.-B., Luo, A. L., Lu, Y.-J., et al., 591 High-velocity Stars in the Galactic Halo Selected from LAMOST DR7 and Gaia DR2. 2021, *Astrophysical Journal, Supplement*, **252**, 3, DOI:10.3847/1538-4365/abc16e
- Liao, J., Du, C., Deng, M., et al., The Origin of High-velocity Stars Considering the Impact of the Large Magellanic Cloud. 2024, *Astronomical Journal*, **167**, 76, DOI:10.3847/1538-3881/ad18c4

- Liu, J. C., Zhu, Z., & Hu, B., Constructing a Galactic coordinate system based on near-infrared and radio catalogs. 2011, *Astronomy and Astrophysics*, **536**, A102, DOI:10.1051/0004-6361/201116947
- Luo, A. L., Zhang, H.-T., Zhao, Y.-H., et al., Data release of the LAMOST pilot survey. 2012, *Research in Astronomy and Astrophysics*, **12**, 1243, DOI:10.1088/1674-4527/12/9/004
- Majewski, S. R., Schiavon, R. P., Frinchaboy, P. M., et al., The Apache Point Observatory Galactic Evolution Experiment (APOGEE). 2017, *Astronomical Journal*, **154**, 94, DOI:10.3847/1538-3881/aa784d
- Marchetti, T., Rossi, E. M., & Brown, A. G. A., Gaia DR2 in 6D: searching for the fastest stars in the Galaxy. 2019, *Monthly Notices of the RAS*, **490**, 157, DOI:10.1093/mnras/sty2592
- Maurya, J., Joshi, Y. C., Elsahoury, W. H., & Sharma, S., Photometric and Kinematic Study of the Open Clusters SAI 44 and SAI 45. 2021, *Astronomical Journal*, **162**, 64, DOI:10.3847/1538-3881/ac0138
- Metzger, M. R., Caldwell, J. A. R., & Schechter, P. L., The Shape and Scale of Galactic Rotation from Cepheid Kinematics. 1998, *Astronomical Journal*, **115**, 635, DOI:10.1086/300198
- Mihalas, D. & Binney, J. 1981, *Galactic astronomy. Structure and kinematics*
- Mihalas, D., Binney, J., & Antonov, V. A., Book-Review - Galactic Astronomy - Structure and Kinematics. 1983, *Astrofizika*, **19**, 505
- Neunteufel, P., Exploring velocity limits in the thermonuclear supernova ejection scenario for hypervelocity stars and the origin of US 708. 2020, *Astronomy and Astrophysics*, **641**, A52, DOI:10.1051/0004-6361/202037792
- Nouh, M. I. & Elsahoury, W. H., Kinematics and Velocity Ellipsoid of Halo Red Giants. 2020, *Astrophysics*, **63**, 179, DOI:10.1007/s10511-020-09624-5
- O'Leary, R. M. & Loeb, A., Production of hypervelocity stars through encounters with stellar-mass black holes in the Galactic Centre. 2008, *Monthly Notices of the RAS*, **383**, 86, DOI:10.1111/j.1365-2966.2007.12531.x
- Oort, J. H., Additional notes concerning the rotation of the galactic system. 1927a, *Bulletin Astronomical Institute of the Netherlands*, **4**, 91
- Oort, J. H., Observational evidence confirming Lindblad's hypothesis of a rotation of the galactic system. 1927b, *Bulletin Astronomical Institute of the Netherlands*, **3**, 275
- Pakmor, R., Kromer, M., Taubenberger, S., & Springel, V., Helium-ignited Violent Mergers as a Unified Model for Normal and Rapidly Declining Type Ia Supernovae. 2013, *Astrophysical Journal, Letters*, **770**, L8, DOI:10.1088/2041-8205/770/1/L8
- Piffl, T., Williams, M., & Steinmetz, M., Kinematics in galactic tidal tails. A source of hypervelocity stars? 2011, *Astronomy and Astrophysics*, **535**, A70, DOI:10.1051/0004-6361/201117474

- Portegies Zwart, S. F., The Characteristics of High-Velocity O and B Stars Which Are Ejected from Supernovae in Binary Systems. 2000, *Astrophysical Journal*, **544**, 437, DOI:10.1086/317190
- Poveda, A., Ruiz, J., & Allen, C., Run-away Stars as the Result of the Gravitational Collapse of Proto-stellar Clusters. 1967, *Boletín de los Observatorios Tonantzintla y Tacubaya*, **4**, 86
- Rockosi, C. M., Lee, Y. S., Morrison, H. L., et al., SEGUE-2: Old Milky Way Stars Near and Far. 2022, *Astrophysical Journal, Supplement*, **259**, 60, DOI:10.3847/1538-4365/ac5323
- Rossi, E. M., Marchetti, T., Cacciato, M., Kuiack, M., & Sari, R., Joint constraints on the Galactic dark matter halo and Galactic Centre from hypervelocity stars. 2017, *Monthly Notices of the RAS*, **467**, 1844, DOI:10.1093/mnras/stx098
- Shen, K. J., Boubert, D., Gänsicke, B. T., et al., Three Hypervelocity White Dwarfs in Gaia DR2: Evidence for Dynamically Driven Double-degenerate Double-detonation Type Ia Supernovae. 2018, *Astrophysical Journal*, **865**, 15, DOI:10.3847/1538-4357/aad55b
- Soubiran, C., Bienaymé, O., & Siebert, A., Vertical distribution of Galactic disk stars. I. Kinematics and metallicity. 2003, *Astronomy and Astrophysics*, **398**, 141, DOI:10.1051/0004-6361:20021615
- Steinmetz, M., Guiglion, G., McMillan, P. J., et al., The Sixth Data Release of the Radial Velocity Experiment (RAVE). II. Stellar Atmospheric Parameters, Chemical Abundances, and Distances. 2020, *Astronomical Journal*, **160**, 83, DOI:10.3847/1538-3881/ab9ab8
- Taylor, M. B., TOPCAT & STIL: Starlink Table/VOTable Processing Software. 2005, in *Astronomical Society of the Pacific Conference Series*, Vol. **347**, *Astronomical Data Analysis Software and Systems XIV*, ed. P. Shopbell, M. Britton, & R. Ebert, 29
- Wang, B. & Han, Z., Companion stars of type Ia supernovae and hypervelocity stars. 2009, *Astronomy and Astrophysics*, **508**, L27, DOI:10.1051/0004-6361/200913326
- Wang, C., Huang, Y., Yuan, H., et al., The Value-added Catalog for LAMOST DR8 Low-resolution Spectra. 2022, *Astrophysical Journal, Supplement*, **259**, 51, DOI:10.3847/1538-4365/ac4df7
- Wang, F., Zhang, H. W., Huang, Y., et al., Local stellar kinematics and Oort constants from the LAMOST A-type stars. 2021, *Monthly Notices of the RAS*, **504**, 199, DOI:10.1093/mnras/stab848
- Xue, X. X., Rix, H. W., Zhao, G., et al., The Milky Way's Circular Velocity Curve to 60 kpc and an Estimate of the Dark Matter Halo Mass from the Kinematics of ~2400 SDSS Blue Horizontal-Branch Stars. 2008, *Astrophysical Journal*, **684**, 1143, DOI:10.1086/589500
- Yan, Y., Du, C., Li, H., et al., Existence of the Metal-rich Stellar Halo and High-velocity Thick Disk in the Galaxy. 2020, *Astrophysical Journal*, **903**, 131, DOI:10.3847/1538-4357/abbd3d

- Yanny, B., Rockosi, C., Newberg, H. J., et al., SEGUE: A Spectroscopic Survey of 240,000 Stars with $g = 14-20$. 2009, *Astronomical Journal*, **137**, 4377, DOI:10.1088/0004-6256/137/5/4377
- Yu, Q. & Madau, P., Kinematics of hypervelocity stars in the triaxial halo of the Milky Way. 2007, *Monthly Notices of the RAS*, **379**, 1293, DOI:10.1111/j.1365-2966.2007.12034.x
- Yu, Q. & Tremaine, S., Ejection of Hypervelocity Stars by the (Binary) Black Hole in the Galactic Center. 2003, *Astrophysical Journal*, **599**, 1129, DOI:10.1086/379546
- Zhao, G., Zhao, Y.-H., Chu, Y.-Q., Jing, Y.-P., & Deng, L.-C., LAMOST spectral survey — An overview. 2012, *Research in Astronomy and Astrophysics*, **12**, 723, DOI:10.1088/1674-4527/12/7/002
- Zubovas, K., Wynn, G. A., & Gualandris, A., Supernovae in the Central Parsec: A Mechanism for Producing Spatially Anisotropic Hypervelocity Stars. 2013, *Astrophysical Journal*, **771**, 118, DOI:10.1088/0004-637X/771/2/118

A. Special Signs

You may wish to use special signs. A large number of the latter are listed in the *L^AT_EX User's Guide & Reference Manual* by Leslie Lamport, pp. 44 ff. We have created further symbols for math mode, and some special Slovak characters (used e.g. in names), which cannot be simply produced by L^AT_EX.

Table 6. Special signs

Input	Explanation	Output	Input	Explanation	Output
<code>\la</code>	less or approx	\lesssim	<code>\ga</code>	greater or approx	\gtrsim
<code>\getsto</code>	gets over to	$\xrightarrow{\text{to}}$	<code>\cor</code>	corresponds to	\ni
<code>\lid</code>	less or equal	\leq	<code>\gid</code>	greater or equal	\geq
<code>\sol</code>	similar over less	\lesssim	<code>\sog</code>	similar over greater	\gtrsim
<code>\lse</code>	less over simeq	\lesssim	<code>\gse</code>	greater over simeq	\gtrsim
<code>\grole</code>	greater over less	\gtrsim	<code>\leogr</code>	less over greater	\lesssim
<code>\loa</code>	less over approx	\lesssim	<code>\goa</code>	greater over approx	\gtrsim
<code>\degr</code>	degree	$^{\circ}$			
<code>\diameter</code>	diameter	\bigcirc	<code>\sq</code>	square	\square
<code>\fd</code>	fraction of day	d	<code>\fh</code>	fraction of hour	h
<code>\fm</code>	fraction of minute	m	<code>\fs</code>	fraction of second	s
<code>\fdg</code>	fraction of degree	$^{\circ}$	<code>\fp</code>	fraction of period	P
<code>\farcs</code>	fraction of arcsecond	$''$	<code>\farcm</code>	fraction of arcmin	$'$
<code>\arcsec</code>	arcsecond	$''$	<code>\arcmin</code>	arcminute	$'$
<code>\angstrom</code>	ångström	Å			
<code>\softL</code>	Slovak L with caron	Ľ	<code>\softl</code>	Slovak l with caron	ĺ
<code>\softd</code>	Slovak d with caron	ď	<code>\softt</code>	Slovak t with caron	ť